DOI: 10.1002/chem.200500434

Interplay between Intra- and Interligand Charge Transfer with Variation of the Axial N-Heterocyclic Ligand in Osmium(II) Pyridylpyrazolate Complexes: Extensive Color Tuning by Phosphorescent Solvatochromism

Shih-Wen Li,[a] Yi-Ming Cheng,[a] Yu-Shan Yeh,[a] Cheng-Chih Hsu,[a] Pi-Tai Chou,*[a] Shie-Ming Peng,[a] Gene-Hsiang Lee,[a] Yung-Liang Tung,[b] Pei-Chi Wu,[b] Yun Chi,*[b] Fang-Iy Wu,[c] and Ching-Fong Shu*[c]

Abstract: The rational design and syntheses of a new series of Os^{II} complexes with formula $[Os(fppz)_2(CO)(L)]$ (**1**: L = 4-dimethylaminopyridine; **2**: L = pyridine; **3**: L = 4,4′-bipyridine; **4**: L = pyridazine; **5**: L = 4-cyanopyridine), bearing two (2-pyridyl)pyrazolate ligands (fppz) together with one carbonyl and one N-heterocyclic ligand at the axial positions are reported. Single-crystal X-ray diffraction studies of, for example, **2** reveal a distorted octahedral geometry in which both fppz ligands reside in the equatorial plane with a *trans* configuration and adopt a bent arrangement at the metal center with a dihedral angle of ~23°, while the carbonyl and pyridine ligands are located at the axial positions. Variation of the axial N-heterocyclic ligand leads to remarkable changes in the photophysical properties as the energy gap and hence the phosphorescence peak wavelength can be tuned. For complexes **1** and **2** the solvent-polarity-independent phosphorescence originates from a combination of intraligand $^3\pi$–π^* (^{3}ILCT) and metal-to-ligand charge transfer transitions (^{3}MLCT). In sharp contrast, as supported by cyclic voltammetry measurements and theoretical calculations, complexes **3**–**5** exhibit mainly ligand-to-ligand charge transfer (LLCT) transitions, resulting in a large dipolar change. The phosphorescence of complexes **3**–**5** thus exhibits a strong dependence on the polarity of the solvent, being shifted for example, from 560 (in C_6H_{12}) to 665 nm (in CH_3CN) and from 603 (in C_6H_{12}) to 710 nm (in CH_3CN) for complexes **3** and **5**, respectively. The results clearly demonstrate that a simple, straightforward derivatization of the axial N-heterocyclic ligand drastically alters the excitation properties per se from intraligand charge transfer (ILCT) to LLCT transitions. The latter exhibit remarkable LLCT phosphorescence solvatochromism so that a broad range of color tunability can be achieved.

Keywords: charge transfer · N ligands · osmium · phosphorescence · solvatochromism

Introduction

Recently, much effort has been directed towards the synthesis and characterization of octahedral iridium complexes with specially tailored cyclometalated ligands.[1] These complexes have attracted much attention because of their high luminescence quantum yields and long-lived excited states caused by efficient intersystem crossing from the singlet to the triplet excited states. These properties increase the potential of these complexes in applications such as oxygen sensors[2] and as the emissive dopants in phosphorescent organic light-emitting devices (OLEDs).[3] Devices based on these materials may have an electroluminescent efficiency that is theoretically four times greater than that of fluorescent dopants, for which an upper limit of about 25% of electron and hole recombination would produce the required

[a] S.-W. Li, Y.-M. Cheng, Y.-S. Yeh, C.-C. Hsu, Prof. Dr. P.-T. Chou, Prof. Dr. S.-M. Peng, G.-H. Lee
Department of Chemistry and Instrumentation Center
National Taiwan University, Taipei 106 (Taiwan)
Fax: (+886) 223-695-208
E-mail: chop@ntu.edu.tw

[b] Y.-L. Tung, P.-C. Wu, Prof. Dr. Y. Chi
Department of Chemistry, National Tsing Hua University, Hsinchu 300 (Taiwan)
Fax: (+886) 357-20-864
E-mail: ychi@mx.nthu.edu.tw

[c] F.-I. Wu, Prof. Dr. C.-F. Shu
Department of Applied Chemistry, National Chiao Tung University
Hsinchu 300, Taiwan
Fax: (+886) 357-23-764
E-mail: shu@cc.nctu.edu.tw

emission through the population of the singlet excited states.[4]

More recently, these investigations have been extended to the isoelectronic osmium(II) complexes.[5] Neutral complexes of formula $[Os(fppz)_2L_2]$[6] are a particularly important class of luminescent osmium(II) complexes, where "fppz" stands for 3-trifluoromethyl-5-(2-pyridyl)pyrazole and L denotes the π-acidic carbonyl ligand or even more electron-donating ligands such as PPh_2Me and $PPhMe_2$. These carbonyl derivatives possess two orthogonal fppz ligands, leaving the carbonyl ligands to adopt a *cis* orientation in which the competition for the metal π electron can be minimized. Moreover, this complex exhibits a bright blue emission from the ligand-centered $^3\pi\pi^*$ excited state.[6a] After phosphine substitution, the fppz chelates undergo ligand reorientation, giving rise to an all-*trans* and planar conformation. The emission signal is also red-shifted to the longer wavelength range of 620–650 nm depending on the electron-donating or π-accepting capability of the phosphine utilized.[6b] This observation clearly demonstrates that by tuning the energetics of osmium(II) metal d_π orbitals the emitting state alters from the ligand-centered $^3\pi\pi^*$ state to the metal-to-ligand charge transfer state (^{3}MLCT). Further investigations of the luminescent behavior of other types of charge-neutral $[Os(fppz)_2L_2]$ complexes are thus of great importance from both fundamental and application points of view.

Herein, we report the characteristics of a new series of osmium(II) metal complexes **1**–**5** bearing two (2-pyridyl)pyrazolate ligands together with one carbonyl and one functionalized N-heterocyclic donor ligand at the mutually *trans* axial positions (see Scheme 1). The results shown in the following sections clearly demonstrate that a simple derivatization of the axial N-heterocyclic donor is capable of converting the excitation properties from intraligand to ligand-to-ligand (interligand) transitions. For the interligand charge transfer transition, as a result of the large changes in the dipolar vectors compared with those of the ground state, remarkable phosphorescence solvatochromism was observed, leading to an exceedingly broad range of color tunability.

Experimental Section

General information and materials: Mass spectra were obtained on a JEOL SX-102A instrument operating in electron-impact (EI) or fast-atom-bombardment (FAB) mode. ^{1}H and ^{13}C NMR spectra were recorded with a Varian Mercury-400 or INOVA-500 instrument; for both ^{1}H and ^{13}C NMR spectra, chemical shifts are quoted with respect to the internal standard tetramethylsilane. Elemental analyses were carried out at the NSC Regional Instrumentation Center at National Chiao Tung University, Hsinchu, Taiwan. All reactions were performed under nitrogen using anhydrous solvents or solvents treated with an appropriate drying reagent. The progress of the reactions was monitored by using Merck TLC plates precoated with fluorescent indicator UV_{254}. Column chromatography was carried out by using silica gel purchased from Merck (230–400 mesh).

Preparation of $[Os(fppz)_2(CO)(npy)]$ (1): A stirred solution of $[Os(fppz)_2(CO)_2]$ (120 mg, 0.179 mmol) in anhydrous ethanol (15 mL) was treated dropwise with an ethanolic solution (10 mL) of freshly sublimed Me_3NO (20 mg, 0.268 mmol) under nitrogen at room temperature over a period of 5 min. The stirring was continued for 10 min, after which 4-dimethylaminopyridine (npy, 66 mg, 0.537 mmol) was added and the solution was refluxed for 20 h, during which time the solution gradually changed from milky white to pale yellow and finally to yellow. The desired yellow crystalline product $[Os(fppz)_2(CO)(npy)]$ was obtained by slowly cooling the reaction mixture to room temperature and was then collected by filtration (93 mg, 0.122 mmol, 68%). Further purification was conducted by recrystallization from a mixture of CH_2Cl_2 and hexane at room temperature.

Spectral data of **1**: ^{1}H NMR (400 MHz, [D$_6$]acetone, 25°C): $\delta = 10.65$ (d, J(H,H) = 5.6 Hz, 2H), 8.04–7.94 (m, 4H), 7.53–7.45 (m, 4H), 7.16 (s, 2H), 6.22 (d, J(H,H) = 7.2 Hz, 2H), 2.81 ppm (s, 6H); ^{13}C NMR (125 MHz, [D$_6$]acetone): $\delta = 174.4$ (CO), 158.3 (2 C), 155.3 (2 CH), 155.0 (C), 153.5 (2 C), 147.5 (2 CH), 143.0 (q, ^2J(C,F) = 35.5 Hz, 2 C), 139.1 (2 CH), 123.4 (q, ^1J(C,F) = 265.0 Hz; 2 CF_3), 123.1 (2 CH), 119.6 (2 CH), 107.6 (2 CH), 103.0 (2 CH), 38.7 ppm (NMe_2); ^{19}F NMR (470 MHz, [D$_6$]acetone): $\delta = -59.67$ ppm (s, CF_3); IR (CH_2Cl_2): $\tilde{\nu} = 1914\ cm^{-1}$ (C=O); MS (FAB, ^{192}Os): m/z: 766 [M^+], 738 [$Os(fppz)_2(npy)^+$], 644 [$Os(fppz)_2(CO)^+$], 616 [$Os(fppz)_2^+$]; elemental analysis calcd (%) for $C_{23}H_{20}F_6N_8OOs$: C 40.84, N 14.65, H 2.64; found: C 40.30, N 14.22, H 2.89.

Preparation of $[Os(fppz)_2(CO)(py)]$ (2): A stirred solution of $[Os(fppz)_2(CO)_2]$ (102 mg, 0.152 mmol) in anhydrous ethanol (15 mL) was treated dropwise with an ethanolic solution (3 mL) of freshly sublimed Me_3NO (17 mg, 0.228 mmol) under nitrogen at room temperature over a period of 5 min. The stirring was continued for 10 min and then pyridine (py, 37 μL, 0.455 mmol) was added to this mixture and the solution was refluxed for 4 h, during which time the solution gradually changed from milky white to light yellow and finally to orange. The solvent was then removed under vacuum, the residue was taken into ethyl acetate (35 mL), and the solution was washed with deionized water three times (20 mL × 3). The organic phase was dried with anhydrous Na_2SO_4 and the filtrate was concentrated to dryness to give an orange solid. This crude product was then loaded onto a silica gel column and eluted with a mixture of ethyl acetate and hexane (1:1). Finally, the desired compound $[Os(fppz)_2(CO)(py)]$ was recrystallized from an CH_2Cl_2 and hexane mixture to give yellow crystals (67 mg, 0.091 mmol, 60%).

Spectral data of **2**: ^{1}H NMR (500 MHz, [D$_6$]acetone, 25°C): $\delta = 10.60$ (dd, J(H,H) = 5.8, 1.5 Hz, 2H), 8.14 (dd, J(H,H) = 5.2, 1.5 Hz, 2H), 8.04 (ddd, J(H,H) = 7.3, 5.8, 1.5 Hz, 2H), 7.94 (dd, J(H,H) = 7.3, 5.8 Hz, 2H), 7.74 (td, J(H,H) = 7.4, 1.5 Hz, 1H), 7.56 (ddd, J(H,H) = 7.3, 5.8, 1.5 Hz, 2H), 7.23 (ddd, J(H,H) = 7.4, 5.2, 1.5 Hz, 2H), 7.16 ppm (s, 2H); ^{13}C NMR (125 MHz, [D$_6$]acetone, 25°C): $\delta = 174.8$ (CO), 158.4 (2 C), 155.6 (2 CH), 153.8 (2 C), 149.5 (2 CH), 143.7 (q, ^2J(C,F) = 35.5 Hz, 2 C), 140.1 (CH), 139.8 (2 CH), 126.6 (2 CH), 123.9 (2 CH), 123.6 (q, ^1J(C,F) = 265.5 Hz, 2 CF_3), 120.1 (2 CH), 103.5 ppm (2 CH); ^{19}F NMR (470 MHz, [D$_6$]acetone, 25(C): $\delta = -59.90$ ppm (s, CF_3); IR (CH_2Cl_2): $\tilde{\nu} = 1931\ cm^{-1}$ (C=O); MS (FAB, ^{192}Os): m/z: 723 [M^+], 616 [$Os(fppz)_2^+$]; elemental analysis calcd (%) for $C_{24}H_{15}F_6N_7OOs$: C 39.94, N 13.59, H 2.10; found: C 39.85, N 13.72, H 2.32.

Preparation of $[Os(fppz)_2(CO)(4bpy)]$ (3): Following procedures identical to those used in the preparation of **2**, using the Os complex $[Os(fppz)_2(CO)_2]$ (101 mg, 0.150 mmol), freshly sublimed Me_3NO (17 mg, 0.225 mmol), and 4,4′-bipyridine (4bpy, 70 mg, 0.45 mmol) in anhydrous ethanol (ca. 20 mL). Orange crystals of $[Os(fppz)_2(CO)(4bpy)]$ (**3**) (42 mg, 0.053 mmol, 35%) were obtained by column chromatography using a 1:1 mixture of hexane and ethyl acetate followed by crystallization from a mixture of ethyl acetate and hexane at room temperature. Complex **3** is somewhat unstable in chlorinated solvents such as CH_2Cl_2, giving a dark brown solution within a period of 4 h.

Spectral data of **3**: ^{1}H NMR (400 MHz, $CDCl_3$, 25°C): $\delta = 10.56$ (d, J(H,H) = 5.6 Hz, 2H), 8.63 (d, J(H,H) = 6.0 Hz, 2H), 8.20 (d, J(H,H) = 5.4 Hz, 2H), 7.77 (dd, J(H,H) = 8.0, 6.8 Hz, 2H), 7.56 (d, J(H,H) = 8.0 Hz, 2H), 7.37–7.32 (m, 4H), 7.23 (dd, J(H,H) = 5.6, 6.8 Hz, 2H), 6.88 ppm (s, 2H); ^{13}C NMR (125 MHz, [D$_6$]acetone, 25°C): $\delta = 174.8$ (CO), 158.5 (2 C), 155.7 (2 CH), 153.9 (2 C), 151.6 (2 CH), 150.2 (2 CH), 148.7 (C), 143.9 (q, ^2J(C,F) = 35.5 Hz, 2 C), 143.4 (C), 139.8 (2 CH), 124.1 (2 CH), 123.9 (2 CH), 123.6 (q, ^1J(C,F) = 266.1 Hz, 2 CF_3), 122.0 (2 CH), 120.2 (2

CH), 103.6 ppm (2 CH); ^{19}F NMR (470 MHz, [D$_6$]acetone, 25 °C): $\delta = -59.80$ ppm (s, CF$_3$); IR (CH_2Cl_2): $\tilde{\nu} = 1933\ cm^{-1}$ (C=O); MS (FAB, ^{192}Os): m/z: 800 [M^+], 772 [Os(fppz)$_2$(4bpy)$^+$], 644 [Os(fppz)$_2$(CO)$^+$], 616 [Os(fppz)$_2^+$]; elemental analysis calcd (%) for $C_{29}H_{18}F_6N_8OOs$: C 43.61, N 14.03, H 2.27; found: C 44.01, N 13.69, H 2.48.

Preparation of [Os(fppz)$_2$(CO)(pyd)] (4): Following procedures identical to those used in the preparation of **2**, using the Os complex [Os(fppz)$_2$(CO)$_2$] (107 mg, 0.159 mmol), freshly sublimed Me_3NO (18 mg, 0.239 mmol), and pyridazine (pyd, 34 μL, 0.477 mmol) in anhydrous ethanol (ca. 20 mL). [Os(fppz)$_2$(CO)(pyd)] (**4**) (40 mg, 0.056 mmol, 35 %) was obtained as an orange crystalline solid by column chromatography using hexane and ethyl acetate (1:2) followed by crystallization from a mixture of CH_2Cl_2 and hexane at room temperature.

Spectral data of **4**: ^{1}H NMR (400 MHz, [D$_6$]acetone, 25 °C): $\delta = 10.63$ (d, J(H,H) = 5.8 Hz, 2H), 8.80–8.78 (m, 1H), 8.69–8.67 (m, 1H), 8.02 (dd, J(H,H) = 6.3, 7.6 Hz, 2H), 7.94 (d, J(H,H) = 7.6 Hz, 2H), 7.65 (t, J(H,H) = 3.8 Hz, 2H), 7.50 (dd, J(H,H) = 5.8, 6.3 Hz, 2H), 7.12 ppm (s, 2H); ^{13}C NMR (125 MHz, [D$_6$]acetone, 25 °C): $\delta = 175.6$ (CO), 158.7 (2 C), 156.3 (2 CH), 153.6 (CH), 153.5 (2 C), 153.0 (CH), 143.0 (q, ^2J(C,F) = 35.5 Hz, 2 C), 139.5 (2 CH), 131.5 (CH), 130.3 (CH), 123.3 (2 CH), 123.9 (q, ^1J(C,F) = 266.1 Hz, 2 CF$_3$), 119.7 (2 CH), 103.1 ppm (2 CH); ^{19}F NMR (470 MHz, [D$_6$]acetone, 25 °C): $\delta = -59.66$ ppm (s, CF$_3$); IR (CH_2Cl_2): $\tilde{\nu} = 1922\ cm^{-1}$ (C=O); MS (FAB, ^{192}Os): m/z: 724 [M^+], 696 [Os(fppz)$_2$(pyd)$^+$], 644 [Os(fppz)$_2$(CO)$^+$], 616 [Os(fppz)$_2^+$]; elemental analysis calcd (%) for $C_{23}H_{14}F_6N_8OOs$: C 38.23, N 15.51, H 1.95; found: C 37.50, N 15.10, H 2.20.

Preparation of [Os(fppz)$_2$(CO)(cpy)] (5): Following procedures identical to those used in the preparation of **2**, using the Os complex [Os(fppz)$_2$(CO)$_2$] (104 mg, 0.155 mmol), freshly sublimed Me_3NO (17 mg, 0.232 mmol), and 4-cyanopyridine (cpy, 48 mg, 0.465 mmol) in anhydrous ethanol (20 mL). Orange crystals of [Os(fppz)$_2$(CO)(cpy)] (**5**) (32 mg, 0.043 mmol, 28 %) were obtained from by chromatography using hexane and ethyl acetate (1:1) and crystallization from a mixture of CH_2Cl_2 and hexane at room temperature.

Spectral data of **5**: ^{1}H NMR (400 MHz, [D$_6$]acetone, 25 °C): $\delta = 10.58$ (dd, J(H,H) = 6.0, 1.2 Hz, 2H), 8.41 (dd, J(H,H) = 5.4, 1.8 Hz, 2H), 8.05 (ddd, J(H,H) = 6.0, 7.6, 1.2 Hz, 2H), 7.97 (d, J(H,H) = 7.6 Hz, 2H), 7.70 (dd, J(H,H) = 5.4, 1.8 Hz, 2H), 7.59 (ddd, J(H,H) = 7.6, 6.0, 1.2 Hz, 2H), 7.14 ppm (s, 2H); ^{13}C NMR (125 MHz, [D$_6$]acetone, 25 °C): $\delta = 174.8$ (CO), 158.3 (2 C), 155.6 (2 CH), 153.9 (2 C), 150.9 (2 CH), 143.8 (q, ^2J(C,F) = 35.5 Hz, 2 C), 140.0 (2 CH), 128.9 (2 CH), 124.1 (2 CH), 122.4 (q, ^1J(C,F) = 263.5 Hz, 2 CF$_3$), 123.6 (C), 120.2 (2 CH), 115.9 (CN), 103.7 ppm (2 CH); ^{19}F NMR (470 MHz, [D$_6$]acetone, 25 °C): $\delta = -59.83$ ppm (s, CF$_3$); IR (CH_2Cl_2): $\tilde{\nu} = 1938\ cm^{-1}$ (C=O); MS (FAB, ^{192}Os): m/z: 748 [M^+], 720 [Os(fppz)$_2$(cpy)$^+$], 644 [Os(fppz)$_2$(CO)$^+$], 616 [Os(fppz)$_2^+$]; elemental analysis calcd (%) for $C_{25}H_{14}F_6N_8OOs$: C 40.22, N 15.01, H 1.89; found: C 40.51, N 14.87, H 2.02.

Measurements: Single-crystal X-ray analysis was performed with a Bruker SMART Apex CCD diffractometer using $Mo_{K\alpha}$ radiation ($\lambda = 0.71073$ Å). The data collection was executed using the SMART program. Cell refinement and data reduction were carried out using the SAINT program. The structure was determined using the SHELXTL/PC program and refined by using full-matrix least-squares methods. All non-hydrogen atoms were refined anisotropically, whereas hydrogen atoms were placed at the calculated positions and included in the final stage of the refinement with fixed parameters. The crystallographic refinement parameters of complex **2** are summarized in Table 1 and selected bond lengths and angles are listed in Table 2.

CCDC-271969 contains the supplementary crystallographic data for this paper. These data can be obtained free of charge from the Cambridge Crystallographic Data Centre via www.ccdc.cam.ac.uk/data_request/cif.

Cyclic voltammetry (CV) measurements were performed by using a BAS 100 B/W electrochemical analyzer. The oxidation and reduction measurements were recorded, respectively, in anhydrous CH_2Cl_2 and anhydrous THF containing 0.1 M $TBAPF_6$ as the supporting electrolyte at a scan rate of 100 mV s^{-1}. The potentials were measured against an Ag/Ag$^+$ (0.01 M $AgNO_3$) reference electrode with ferrocene as the internal standard.

Table 1. X-ray structural data of complex **2**.

formula	$C_{24}H_{15}F_6N_7OOs$
M_r	721.63
crystal system	triclinic
space group	$P\bar{1}$
T [K]	295(2)
a [Å]	8.9216(5)
b [Å]	9.6844(5)
c [Å]	14.8374(8)
α [°]	86.458(1)
β [°]	89.951(1)
γ [°]	78.293(1)
V [Å^3]	1252.8(1)
Z	2
ρ_{calcd} [g cm^{-3}]	1.913
$F(000)$	692
$\mu(Mo_{K\alpha})$ [mm^{-1}]	5.167
crystal size [mm]	0.17 × 0.15 × 0.12
h, k, l ranges	−11, 11; −12, 12; −19, 19
transmission: max, min.	0.5760, 0.4737
data/restraints/parameters	5760/0/352
GOF on F^2	1.152
R_1, wR_2 with $I > 2\sigma(I)$	0.0348, 0.0760
D-map, max/min^{-1} [e Å^{-3}]	1.225/−1.011

Table 2. Selected bond lengths [Å] and angles [°] for complex **2**.

Os−C1	1.835(6)	Os−N1	2.100(4)
Os−N2	2.060(4)	Os−N4	2.096(4)
Os−N5	2.060(4)	Os−N7	2.186(4)
O1−C1	1.153(7)	C2···N6	3.268
H2A···N6	2.483	C11···N3	3.248
H11A···N3	2.471		
C1-Os-N7	179.6(2)	N1-Os-N2	76.9(2)
N4-Os-N5	76.9(2)	N1-Os-N5	102.5(2)
N2-Os-N4	102.4(2)		

Steady-state absorption and emission spectra were recorded with a Hitachi (U-3310) spectrophotometer and an Edinburgh (FS920) fluorimeter, respectively. Quinine sulfate with an emission yield of $\Phi \sim 0.57$ in 0.1 M H_2SO_4 served as the standard to calculate the emission quantum yield. The degassed samples were prepared by three freeze–pump–thaw cycles under vacuum ($\sim 10^{-5}$ Torr). Nanosecond lifetime studies were performed with an Edinburgh FL 900 photon-counting system. The emission decays were analyzed by the sum of exponential functions, which allows partial removal of the instrument time-broadening and consequently renders a temporal resolution of about 200 ps.

Computational methodology: All calculations were performed with the Gaussian 03 package.[7] Geometrical optimization of the electronic ground state was carried out by using the hybrid Hartree–Fock/density functional theory (HF/DFT) method, B3LYP.[8,9] The "double-ζ" quality basis set consisting of Hay and Wadt's effective core potentials (LANL2DZ)[10,11] was employed for osmium element and the 6-31G* basis set[12] for hydrogen, carbon, nitrogen, fluorine, and oxygen atoms. A relativistic effective core potential (ECP) replaced the inner-core electrons of osmium(II), leaving the outer-core ($5s^25p^6$) and valence ($5d^6$) electrons. Time-dependent DFT (TDDFT) calculations were then performed with the same functional and basis set at the optimized geometry to obtain electronic transition energies. Oscillator strengths were deduced from the dipole transition matrix elements (for singlet states only). In the Onsager solvent reaction field model, we applied the Hartree–Fock method with 6-31G(d′, p′) basis sets to calculate the molecular volume, which is defined as the electron density inside a contour of 0.001 electrons bohr^{-3}. Furthermore, as recommended by the Gaussian 03 package, the radius was selected to be 0.5 Å larger than that deduced from the computed volume.

Results and Discussion

Synthesis and characterization: The general approach to the synthesis of the required osmium(II) complexes involved the treatment of the parent carbonyl complex $[Os(fppz)_2(CO)_2]$ with the respective functionalized pyridine ligands in the presence of excess anhydrous Me_3NO (Scheme 1). The

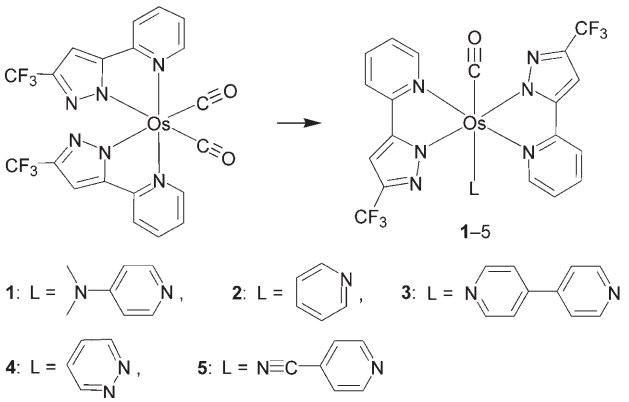

Scheme 1. Synthesis of complexes **1**–**5**.

products prepared by this method consist of monosubstituted derivatives of formula $[Os(fppz)_2(CO)L]$; their formation is independent of the amount of N-heterocyclic donor and Me_3NO reagent added to the reaction mixture. This result is clearly different from the analogous reactions of $[Os(fppz)_2(CO)_2]$ and phosphorus donors in that the latter mainly give disubstituted complexes $[Os(fppz)_2P_2]$, where $P = PPh_2Me$, $PPhMe_2$, etc.[6] The marked differences in these reactions lies in the good electron-donating and poor π-accepting strengths of the pyridyl fragment, which results in relatively less stable Os–N(py) bonds. Moreover, the formation of Os–N bonds may increase the electron density at the osmium d orbitals, strengthening the remaining Os–CO bond interaction and hence reducing the CO bond strength as well. This viewpoint is further confirmed by the observed solution IR ν(CO) stretching signals; **1**: 1914 cm^{-1}; **2**: 1931 cm^{-1}; **3**: 1933 cm^{-1}; **4**: 1922 cm^{-1}; **5**: 1938 cm^{-1}. The trend in the CO stretching frequencies (**1** < **4** < **2**–**3** < **5**) shows a good qualitative correlation with the decrease in the basicity (p*K*) of the free N-heterocyclic ligands; npy: 9.76; py: 5.17; 4bpy: 4.82, pyd: 2.33; cpy: 1.9 (**1** > **2** ~ **3** > **4** > **5**).[13] The only exception is the pyridazine complex **4**, for which the electrostatic repulsion between the vicinal nitrogen atoms would further enhance its electron-donating capability to the osmium(II) cation thereby lowering the observed ν(CO) stretching frequency.[14] Moreover, several attempts were also made to prepare other diazine complexes involving pyrimidine or pyrazine. However, owing to their substantially lower basicities (p*K* of pyrimidine = 1.10 and p*K* of pyrazine = 0.37), a result of the lack of electrostatic repulsion between the vicinal nitrogen atoms compared with that in pyridazine,[14] their reactivities would be lower or the hypothetical reaction products $[Os(fppz)_2(CO)L]$ (L = pyrimidine or pyrazine) less stable with rapid decomposition induced by the loss of the N-heterocycle or even CO ligand. Finally, it is also possible that the postulated disubstituted derivatives $[Os(fppz)_2L_2]$, where L is any one of the N-heterocyclic donors, did exist. However, they would also be relatively unstable and easily give rise to the formation of intractable products.

These osmium complexes were fully characterized using routine NMR spectroscopic methods, while the pyridine complex **2** was further examined by single-crystal X-ray diffraction analysis to establish their exact structure in the solid state. As depicted in Figure 1, complex **2** consists of a

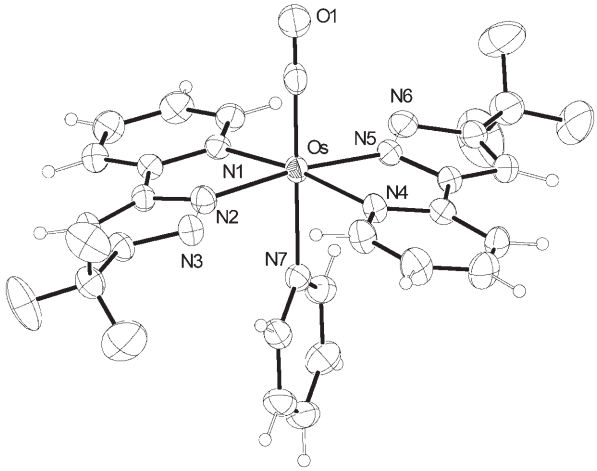

Figure 1. Structure of complex **2** (ORTEP diagram with thermal ellipsoids shown at the 30% probability level).

distorted octahedral configuration around the central osmium(II) atom, with the two chelating fppz ligands located in the equatorial plane, together with the unique carbonyl and the *trans*-pyridine ligands located in the axial positions. The $Os–N_{(py)}$ distance of the axial pyridine ligand is as long as 2.186(4) Å owing to its poor π-bond competition with the CO ligand located *trans* to the pyridine. For the fppz fragments in **2**, the measured $Os–N_{(pz)}$ distances of 2.060(4) Å are slightly shorter than the corresponding $Os–N_{(py)}$ bonds of approximately 2.100(4) Å; however, both bond lengths fall in the range expected for a typical N→osmium(II) dative bond. Of particular interest are the relatively short nonbonding contacts, C(2)···N(6) ~ C(11)···N(3) ~ 3.268 Å and H(2A)···N(6) ~ H(11A)···N(3) ~ 2.48 Å, observed between the *ortho*-substituted C–H fragment of the pyridyl moiety and the nitrogen atom of the nearby pyrazolate fragment. In good agreement with this observation, the ^1H NMR spectrum of **2** revealed a significantly downfield signal at δ = 10.60 ppm, giving additional evidence for the deshielding effect exerted by the electronegative nitrogen atom. It is speculated that this interligand hydrogen bonding, to a certain extent, is akin to that observed in cobaloxime complexes in which intramolecular hydrogen bonding exists be-

tween the oxygen atoms of the dioxime ligands and gives a downfield ^{1}H NMR chemical shift of $\delta \sim 18.0$ ppm.[15] Moreover, the equatorial fppz ligands adopt a bent arrangement with a large dihedral angle of about 23°, the arrangement of which sharply contrasts the near planar geometry observed in the related diphosphine complexes [Os(fppz)$_2$P$_2$] (P = PPh_2Me, $PPhMe_2$, etc).[6] The driving force that influences the overall chelating ligand arrangement at the metal center remains unknown. However, it is possible that the subtlety of the hydrogen bonding between the fppz ligands play a significant role. On the other hand, it is believed that the crystal-packing effect, in part, should also be important for producing the observed distortion. Intriguingly, however, this distortion is reminiscent of the analogous metalloporphyrin compounds, in which a large saddle distortion of the porphyrin ring structure is observed in the carbonyl complexes [Os(TPP)(CO)L] (L = pyridine and 1-methylimidazole),[16] whilst a planar arrangement is observed for the diphosphine-substituted complexes [Os(TPP)(PPh_3)$_2$] and [Os(OEP)($OPPh_3$)$_2$] (H_2TTP = *meso*-tetraphenylporphyrin and H_2OEP = octaethylporphyrin).[17]

Photophysical properties: As shown in Figure 2, the UV/Vis absorption spectra of complexes **1**–**5** in cyclohexane exhibit similar features. Their absorption peaks were found to have

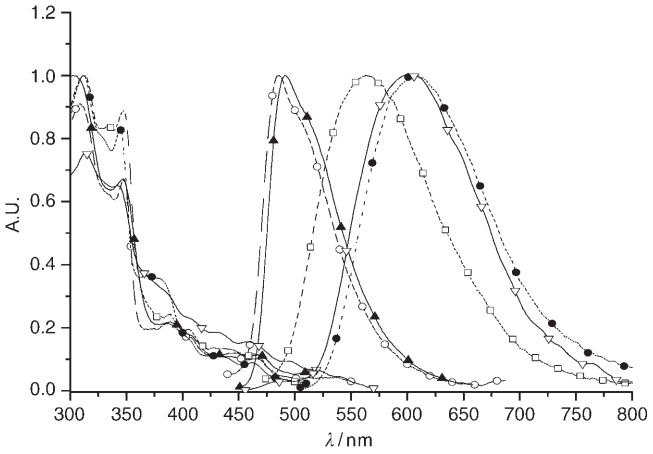

Figure 2. Absorption and emission spectra of complexes **1**–**5** recorded in cyclohexane solution: **1** (▲), **2** (○), **3** (□), **4** (▽), and **5** (●).

large molar extinction coefficients of the order of about 10^4 M^{-1}cm^{-1} (260–350 nm) and were insensitive to solvent polarity. Thus, the dominant absorption bands in the 260–350 nm region were ascribed to ligand-centered $S_0 \rightarrow S_n$ ($n \geq 2$, fppz π–π^*) transitions. In the case of **2**, the lower-lying transition bands at >350 nm, which have relatively weak absorptivity ($\varepsilon < 3000$ M^{-1}cm^{-1}), are mainly ascribed to Os(d_π)-to-pyridyl (in fppz) ligand (MLCT) transitions in combination with pyrazolate-to-pyridyl intraligand π–π^* (ILCT) transitions. In contrast, as supported by theoretical calculations, the lower-lying transitions of complexes **3**–**5** originate primarily from transitions either from Os(d_π) or pyrazolate to the axial N-heterocyclic groups, and are assigned to MLCT or ligand-to-ligand π–π^* transitions (LLCT), respectively, in the singlet state. The lowest absorption bands at >450 nm should incorporate these transitions in the triplet states, which are partially allowed owing to the enhancement of spin–orbit coupling in the osmium(II) atom. However, strong overlapping with bands arising from the singlet states makes the assignment of these peak wavelengths difficult. Detailed insights into the triplet states are elaborated in the section on luminescent and theoretical approaches. The peak wavelengths and extinction coefficients of the first three allowed absorption peaks in various solvents are listed in Table 3.

Despite the similarity in the absorption spectral features, salient differences were resolved in the emission spectra. In a nonpolar solvent such as cyclohexane, in which there is negligible solvent perturbation, the emission peak wavelengths of 497 and 487 nm for **1** and **2**, respectively, are clearly blue shifted in comparison to those of **3** (560 nm), **4** (600 nm), and **5** (603 nm) (see Figure 2). Other photophysical properties such as the emission quantum yields (Φ) and the relaxation kinetic data for **1**–**5** in cyclohexane solution are listed in Table 3. As shown in Table 3 the emission intensities of **1**–**5** are modest, with quantum yields measured to be in the range of 1.0×10^{-3}–1.5×10^{-1} in degassed cyclohexane, while their corresponding emission lifetimes were in the range of a few to several hundred nanoseconds. Accordingly, a radiative decay rate constant, k_r ($=\Phi_{deg}/\tau_{deg}$, see Table 3 for the definition of Φ_{deg} and τ_{deg}) of $\sim10^6$ s^{-1} was deduced for complexes **1**–**5** (e.g., 1.8×10^6 s^{-1} for **1**, 1.3×10^6 s^{-1} for **2**, also see Table 3 for **3**–**5**) in cyclohexane. The radiative lifetime in the μs range, in combination with the significant oxygen quenching (in terms of the signal intensity) and the decay rate constants (see Table 3), lead us to ascertain that the emission from complexes **1**–**5** originates from the triplet state.

The phosphorescence spectra of both complexes **1** and **2** were observed to have very little dependence on the solvent polarity. In the case of **2**, the peak wavelength is red-shifted by only 18 nm by changing the solvent from cyclohexane (487 nm) to acetonitrile (~505 nm, see Table 3). In sharp contrast, remarkably large Stokes-shifted emission was resolved for complexes **3**–**5**. As shown in Figure 3, the phosphorescence of **3** is bathochromically shifted as the polarity of the solvent increases, being shifted from 560 nm in cyclohexane to as high as 665 nm in CH_3CN. Likewise, as depicted in Figure 4 and Figure 5, emission from **4** and **5**, respectively, was found to be significantly dependent on the polarity of the solvent. As the same emission excitation spectra are obtained in each solvent for the wavelengths monitored (500–750 nm, not shown here), it can be ascertained that the emission band originates from a common ground-state species. Furthermore, the excitation spectra, within experimental error, are also effectively identical to the absorption spectra, indicating that the entire phosphorescence results from a common Franck–Condon excited state. Since the absorption peak wavelength exhibits only a slight shift from

Table 3. Photophysical properties of complexes **1–5** in various solvent systems.[a]

(ε [$M^{-1}cm^{-1}$])	λ_{abs} [nm] [nm]	λ_{em}	Φ_{deg}	Φ_{air} [ns]	τ_{deg} [ns]	τ_{air}
1						
C_6H_{12}	390, 415, 445 (N/A)	494	0.021	0.020	11.8	11.3
CH_3CN	396, 422, 445 (1679, 1058, 767)	512	0.012	0.010	6.9	6.7
2						
C_6H_{12}	389, 411, 449 (N/A)	487	0.002	0.002	1.6	1.6
CH_3CN	394, 419, 442 (1689, 1046, 704)	505	0.002	0.002	1.3	1.3
3						
C_6H_{12}	406, 436, 465 (N/A)	560	0.059	0.038	55.1	36.6
C_6H_6	400, 428, 449 (1484, 968, 694)	589	0.057	0.040	60.3	35.8
THF	397, 424, 450 (2231, 1412, 905)	625	0.040	0.021	55.8	34.4
CH_2Cl_2	396, 427, 449 (2072, 1256, 815)	643	0.012	0.011	33.0	27.6
CH_3CN	365, 397, 433 (2447, 1563, 874)	665	0.005	0.004	12.3	9.7
4						
C_6H_{12}	359, 386, 434 (N/A)	600	0.033	0.006	28.9	9.5
C_6H_6	401, 429, 450 (1878, 1353, 1102)	618	0.086	0.018	263.8	57.0
THF	399, 425, 448 (2704, 1856, 1361)	630	0.040	0.010	185.6	48.6
CH_2Cl_2	397, 420, 446 (3228, 2353, 1770)	641	0.028	0.015	136.3	70.7
CH_3CN	396, 420, 443 (2178, 1508, 866)	654	0.010	0.004	82.6	35.5
5						
C_6H_{12}	435, 462, 504 (N/A)	603	0.147	0.044	421.0	64.7
C_6H_6	400, 427, 449 (2785, 1843, 1515)	641	0.048	0.024	82.8	47.3
THF	395, 426, 448 (2561, 1638, 1289)	664	0.009	0.007	25.1	19.4
CH_2Cl_2	397, 425, 449 (2777, 1758, 1351)	678	0.004	0.004	10.6	8.9
CH_3CN	389, 429, 438 (2004, 1270, 955)	710	0.001	0.001	4.4	4.1

[a] Φ_{deg} and τ_{deg} were recorded in solutions degassed with at least three freeze–pump–thaw cycles, while Φ_{air} and τ_{air} were measured using air-saturated solutions.

cyclohexane to acetonitrile (see Table 3), the anomalously large red-shifted phosphorescence observed for complexes **3–5** should be attributed to a large change in the dipolar vector of the T_1 state, such that solvent dipolar relaxation takes place during the $T_1 \rightarrow S_0$ transition, resulting in a distinctive phosphorescence solvatochromism. Since the difference in the $T_1 \rightarrow S_0$ transition between **1** and **2** and **3–5**, according to frontier orbital analyses, is a result of the completely different LUMOs (vide infra), we tentatively conclude that the $T_1 \rightarrow S_0$ transitions in **3–5** are associated with significant ligand-to-ligand charge transfer (LLCT).[18] Firm support of this viewpoint is rendered by the subsequent theoretical calculations as well as by previous studies of osmium(II) cationic complexes $[(bpy)_2Os(CO)L]^{2+}$ (bpy = 2,2′-bipyridine and L = pyridine and benzonitrile).[19] It is apparent that the $Os(d_\pi) \rightarrow bpy(\pi^*)$ transition is of the lowest energy and long-lived, highly luminescent MLCT states are observed for $[(bpy)_2Os(CO)L]^{2+}$; however, when L is replaced by the electron-donating aminobenzonitrile, ^{3}MLCT emission is quenched as ^{3}LLCT is the lowest triplet state.

The observation of phosphorescence solvatochromism is of fundamental interest.[20] For comparison, in view of the solvent-perturbed phosphorescence properties, a few fascinating examples have been reported for several classes of d^8 and d^{10} metal complexes, for which multicolor bright luminescence is not only sensitive to solvent polarity, but also to other factors such as temperature and even concentration.[21] However, in most cases both absorption and emission are affected, that is, the Franck–Condon energy gap is tuned by solvent environment, while emission solvatochromism, in

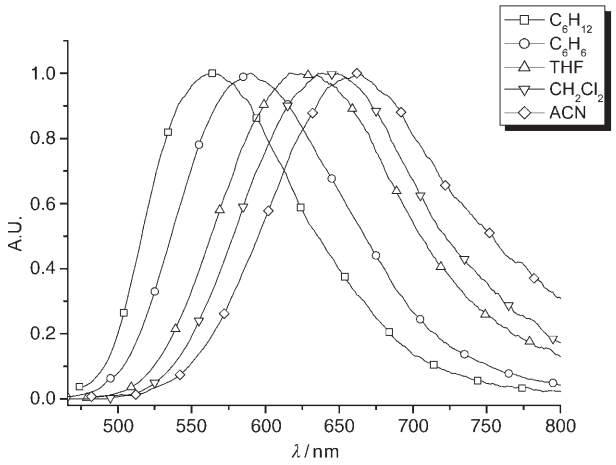

Figure 3. Normalized emission spectra of complex **3** in cyclohexane (□), benzene (○), tetrahydrofuran (△), dichloromethane (▽), and acetonitrile (◇) at room temperature.

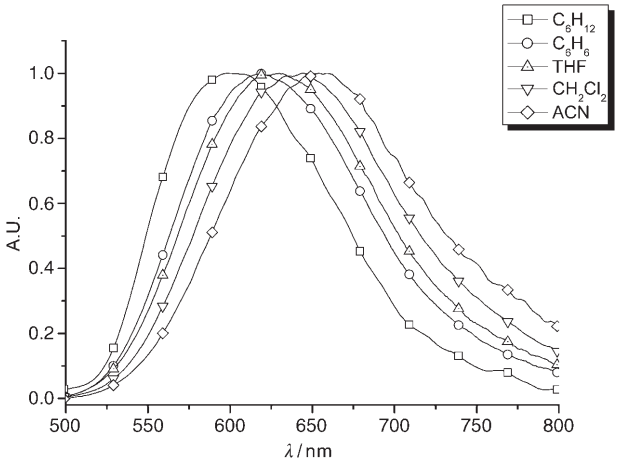

Figure 4. Normalized emission spectra of **4** in cyclohexane (□), benzene (○), tetrahydrofuran (△), dichloromethane (▽), and acetonitrile (◇) at room temperature.

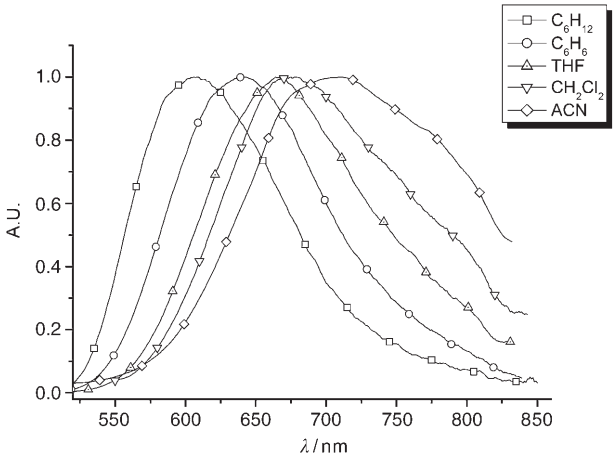

Figure 5. Normalized emission spectra of **5** in cyclohexane (□), benzene (○), tetrahydrofuran (△), dichloromethane (▽), and acetonitrile (◇) at room temperature.

which the phosphorescence is mainly governed by solvent relaxation, is rare. Similar to that deduced from the fluorescence, the dependence of phosphorescence on solvent polarity can be specified quantitatively according to the theory derived from dielectric polarization, which specifies that the spectral shifts of the emission upon increasing solvent polarity depend on the differences in the permanent dipole moments between the ground (S_0) and excited (T_1) states. The magnitude of the excited-state dipole moments can thus be estimated by a method that incorporates the luminescence solvatochromic shift.[22] If the dipole moments of the solute are approximated by a point dipole in the center of a spherical cavity of radius a_0, on the basis of small solvent-dependent absorption properties and negligible solute polarizability, one obtains Equation (1), where $\tilde{\nu}_f$ and $\tilde{\nu}_f^{vac}$ are the spectral positions (in terms of wavenumber) of the solvation-equilibrated fluorescence maxima and the value extrapolated to the diluted gas phase, respectively, $\vec{\mu}_g$ and $\vec{\mu}_e$ are the dipole moment vectors of the ground and excited states, and Δf is the solvent polarity parameter function and is generally expressed as $\Delta f = \frac{\varepsilon-1}{2\varepsilon+1}$, where ε denotes the static dielectric constant of the solvent.

$$\tilde{\nu}_f = \tilde{\nu}_f^{vac} - \frac{2(\vec{\mu}_e - \vec{\mu}_g)^2}{hca_0^3}\Delta f \qquad (1)$$

The plots of the phosphorescence peak frequency as a function of Δf for complexes **3**–**5** are shown in Figure 6. As predicted by Equation (1), a linear relationship is found from cyclohexane to acetonitrile, and slopes as steep as -9427, -4610, and -8111 cm^{-1} were obtained for complexes **3**, **4**, and **5**, respectively, consistent with the assignment of charge-transfer emission. a_0 in Equation (1) was estimated to be 7.3 (**3**), 5.9 (**4**), and 6.7 Å (**5**) by the Hartree–Fock method using 6-31G(d′,p′) basis sets. Accordingly, the change in dipole moment between the ground and excited states was deduced to be as large as 19.08, 9.54, and 15.57 Debye for **3**, **4**, and **5**, respectively.

Electrochemistry: The electrochemical properties of these osmium complexes were investigated by cyclic voltammetry

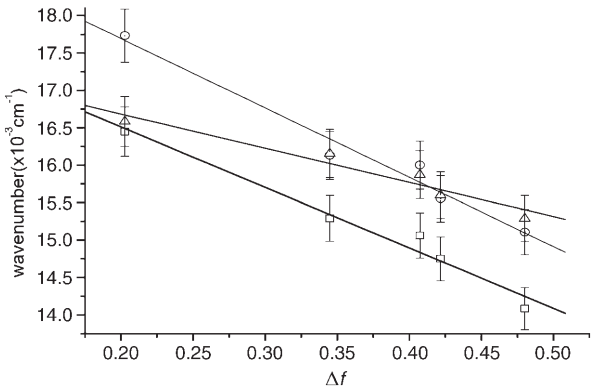

Figure 6. Lippert's plots for complexes **3**–**5**: **3** (○), **4** (△), and **5** (□).

using ferrocene as the internal standard. The results are displayed in Figure 7 and the redox data listed in Table 4. During the anodic scan, all the osmium complexes exhibited

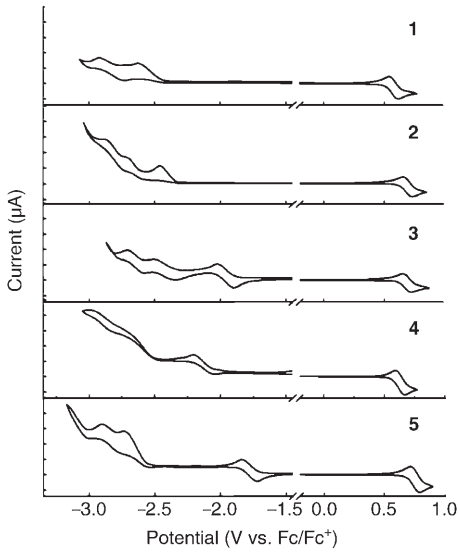

Figure 7. Cyclic voltammograms of the osmium complexes **1**–**5**.

Table 4. Redox potentials of complexes **1**–**5**.

	$E^{ox}_{1/2}$ [V][a]	$E^{red}_{1/2}$ [V][a]
1	0.58	–[b]
2	0.69	−2.46[c]
3	0.69	−1.96
4	0.63	−2.12
5	0.75	−1.78

[a] Potential values referenced versus Fc/Fc^+. [b] No reduction process occurred prior to −2.5 V. [c] Peak potential.

a reversible oxidation wave with potentials in the region of 0.58–0.75 V. It is believed that oxidation mainly occurred at the metal center with a contribution from the cyclometalated pyrazolate fragments. Hence, the formal oxidation potential is strongly dependent on the electronic environment of the osmium(II) cation, that is, good σ-donor and/or poor π-acceptor strengths of the axial N-heterocyclic ligand would shift the oxidative potential to a more negative value. This hypothesis was verified by the effect of an electron-donating dimethylamino group in **1**, which decreased the oxidative potential from 0.69 V for **2** to 0.58 V for **1**, while the electron-withdrawing cyano substituent in complex **5** led to an anodic shift to 0.75 V. However, the replacement of the axial pyridine ligand with a more-conjugated 4,4′-bipyridine ligand in **3** did not significantly change the oxidation potential. For complex **4**, the oxidation potential is cathodically shifted to 0.63 V compared with that of complex **2**. This could be due to pyridazine being a slightly better σ-donor than pyridine, a result possibly originating from the lone pair–lone pair repulsion between the vicinal nitrogen atoms of pyridazine.[14]

The reduction processes are more complicated. They may involve the reduction of either the axial N-heterocyclic ligand or the pyridyl moiety of the fppz ligands. During the cathodic scan, we observed a reversible reduction process for complexes **3**–**5** with potentials in the region of −1.78–−2.12 V, followed by two closely overlapping reductive waves at more negative potentials (ca. −2.6 V). We assigned the first reversible reduction wave to the reduction of the axial N-heterocyclic ligands and the second and third waves to the reduction of the pyridyl sites of the two fppz ligands. For complex **2**, the first reduction peak, which may be related to the reduction of the axial pyridine ligand, was irreversible with the peak potential at −2.46 V and was immediately followed by the reduction peaks of the fppz ligands. On the other hand, we found two irreversible waves for complex **1**, ascribed to the reduction of its two fppz ligands, while the unobserved reduction of the 4-dimethylaminopyridine ligand may occur at a more negative potential. The results of these electrochemical studies show that substituents on the axial ligand significantly affect the redox properties of these osmium complexes. Also, they reveal that the LUMOs in complexes **1** and **2** are mainly located at the pyridyl site of the fppz ligands and are shifted to the N-heterocyclic ligand in complexes **3**–**5**. Qualitatively, this observation is consistent with both the experimental results and the theoretical predictions elaborated as follows.

MO calculations: To gain more insight into the differences in the photophysical properties of **1**–**5**, ab initio calculations (DFT, see Experimental Section) on the molecular orbitals involved in the transitions were carried out. For complexes **1**–**5**, the features of the lowest-unoccupied (LUMO) and the highest-occupied (HOMO) frontier orbitals mainly involved in the low-lying transitions are depicted in Figure 8, while their energy gaps are listed in Table 5. The calculated energies of the lowest triplet states of **1** (468 nm) and **2** (464 nm) are similar in energy to those obtained experimentally (peak wavelengths of 494 nm and 487 nm, respectively) if one neglects the associated vibronic and solvation broadening. Therefore, the level of theory used here is suitable for interpreting the photophysical properties of the complexes concerned. Likewise, the calculated energies of 497 (**3**), 588 (**4**), and 585 nm (**5**) are also qualitatively in agreement with the experimental values (cf. the peak wavelengths in cyclohexane) and are significantly red-shifted compared with complexes **1** and **2**. Indirectly, the results imply differences in the frontier orbitals involved in the transitions, details of which are elaborated as follows.

As shown in Table 5, the lowest energy gap for both singlet and triplet states mainly involves HOMO→LUMO transitions. For complexes **1** and **2**, the electron densities of the HOMOs of the singlet and triplet states are located largely on the $Os(d_\pi)$ and pyrazolate moiety, while the electron densities of the LUMOs are mainly distributed on the pyridyl moiety of the fppz ligands, indicating that the lowest transition involves both a π(pyrazolate)→π*(pyridyl) ILCT and an $Os(d_\pi)$→π*(pyridyl group of fppz) MLCT. As for

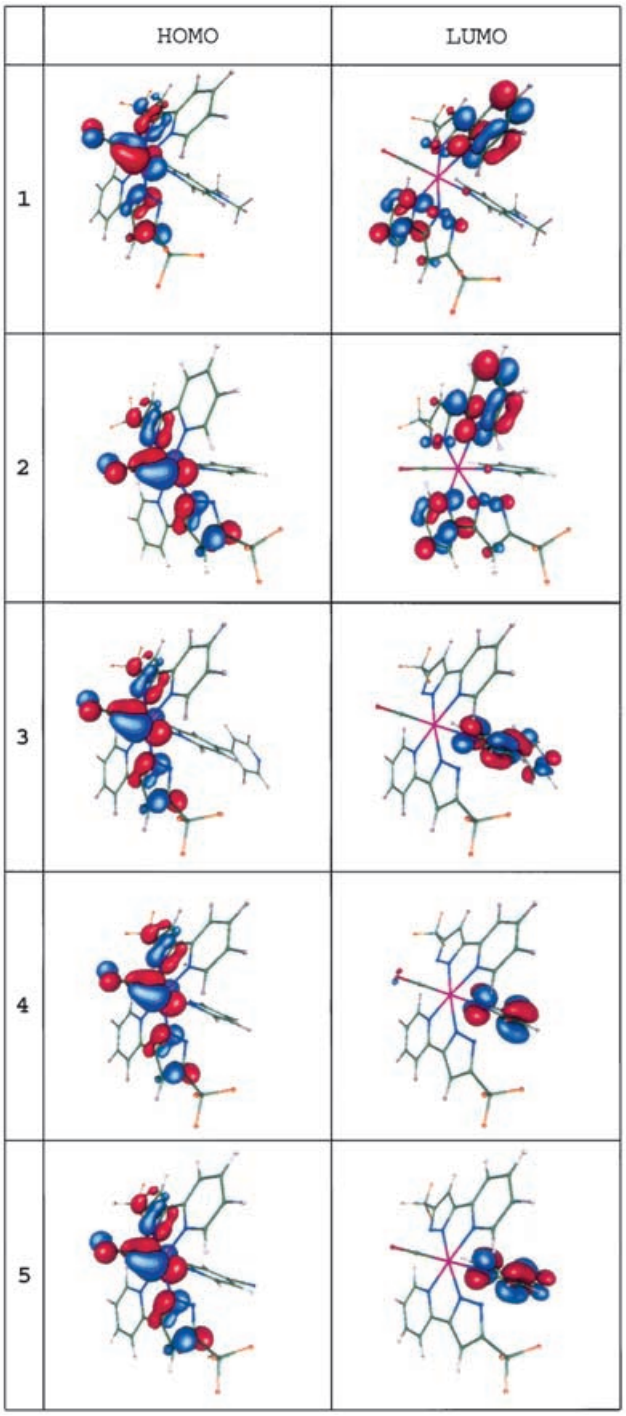

Figure 8. HOMOs and LUMOs of complexes **1**–**5**. Note that the first transition for both singlet and triplet states is dominated by HOMO and LUMO frontier orbitals.

Table 5. The calculated energy levels of the lowest singlet and triplet states of complexes **1**–**5**.

	Transition	Energy gap [eV]	MO contribution	Oscillator strength
1	S_1	2.82 (440)[a]	HOMO→LUMO	0.0147
	T_1	2.65 (468)	HOMO→LUMO	N/A
2	S_1	2.85 (435)	HOMO→LUMO	0.0159
	T_1	2.67 (464)	HOMO→LUMO (95%) HOMO-2→LUMO (5%)	N/A
3	S_1	2.51 (494)	HOMO→LUMO	0.0046
	T_1	2.49 (497)	HOMO→LUMO	N/A
4	S_1	2.16 (574)	HOMO→LUMO	0.0054
	T_1	2.11 (588)	HOMO→LUMO	N/A
5	S_1	2.15 (577)	HOMO→LUMO	0.0035
	T_1	2.12 (585)	HOMO→LUMO	N/A

[a] The unit of the value in the parentheses is nm.

complexes **3**–**5**, although the HOMOs are similar to those of **1** and **2** in terms of electron distribution, in sharp contrast, the electron densities of the LUMOs are exclusively distributed on the axial N-heterocyclic ligand. From the results it can unambiguously be concluded that in addition to MLCT, the lowest $S_0 \rightarrow T_1$ transition for **3**–**5** mainly possesses LLCT character involving π(pyrazolate)→π^*(axial N-heterocyclic ligand) excitation. The resulting LLCT causes huge dipolar change and hence the salient phosphorescence solvatochromism in solution. Among **3**–**5**, the largest dipolar change occurs in **3**, which can be attributed to the longest charge transfer distance (or π conjugation), to the axial 4,4′-bipyridine ligand, of the three complexes. Likewise, the smallest dipolar variation occurs in **4** possessing axial pyridazine, which can be rationalized on the basis of the shortest charge transfer distance. Qualitatively, since the LUMOs of both complexes **1** and **2** are located predominantly at the pyridyl site of fppz, one can safely assume that the reduction potential of the axial pyridine is higher than that of the pyridyl site in fppz, such that the LUMO is exclusively populated at the pyridyl (in fppz) site. The addition of extended π-conjugated or electron-withdrawing substituents, such as the second 4-pyridine group (in **3**), the second in-ring nitrogen atom (to form pyridazine in **4**), and the cyano group (in **5**), should stabilize the lowest π^* level of axial N-heterocyclic ligands.

Consequently, as supported by the theoretical calculations, the LUMO shifts from the pyridyl site of fppz in **1** and **2** to the axial N-heterocyclic ligand in **3**–**5**, and is accompanied by a lowering of the π–π^* transition as well as large dipolar changes due to the alternation of both spatial and orientation features of the dipolar vector. These theoretical predictions are qualitatively in full agreement with both the luminescent and electrochemical properties of **1**–**5** elaborated above. For a comparison, results have recently been reported for a series of iridium complexes with a N^N^N-bonded tpy electron-acceptor (tpy = 2:2′,6′:2″-terpyridine) and a C^N^C-bonded dppy electron-donor ligand (dppy = 2,6-diphenylpyridine); the emitting state of these iridium(III) complexes were unambiguously described as being LLCT in nature.[23] Moreover, LLCT transitions have also been observed in other third-row metal complexes, showing that the emitting excited state has a unique directional character.[24] Further studies have revealed that substituents significantly affect the redox potentials as well as the photophysical properties of complexes. In particular, electron-donating or

π-conjugated substituents on the donor segment reduce the oxidation potential of an orbital that receives significant contributions from the HOMO and leads to LLCT emission from triplet excited states.[25] Conversely, the usual MLCT emission predominates when such a substituent effect is absent.

Conclusions

In conclusion, we have reported the rational design and syntheses of a new series of osmium(II) complexes **1**–**5** bearing two (2-pyridyl)pyrazolate ligands together with one carbonyl and one N-heterocyclic donor at the axial positions. The presence of axial nitrogen-donor ligands as well as the osmium(II) heavy-atom effect makes the photophysical properties of these complexes unique. A straightforward variation of the axial ligand (L) leads to the conversion from ILCT (**1** and **2**) to LLCT (**3**–**5**) emission, with LLCT causing a large change in the dipolar vector. Consequently, a rare room-temperature phosphorescence solvatochromism was observed for complexes **3**–**5**. Thus, **1**–**5**, prepared by a straightforward variation of the axial N-heterocyclic ligand, in solvents of various polarity can achieve extensive broad color tunability from 480 to 720 nm. These results show that coarse-tuning can be achieved by altering the electron-donating/withdrawing properties of the axial N-heterocyclic ligand, while fine-tuning may be manipulated by substituent effects on the planar pyridylpyrazolate ligands.[26] Thus, the design and applications of complexes with multiple hues are feasible and versatile. The results may also spark an interest in designing a solvent-polarity probe as well as a biomolecular probe based on the remarkable phosphorescence solvatochromism. For example, our preliminary results have shown that protonating the dialkylamino group of **1** causes a bathochromic shift from 495 to about 600 nm owing to the loss of the electron-donating property of the dialkylamino group upon protonation. This clearly demonstrates the feasibility of developing a metal-cation sensor based on the analogs of complex **1**. Work on these issues is currently in progress.

Acknowledgements

We thank the National Science Council and the Ministry of Education of Taiwan for financial support of this work.

[1] a) J. Li, P. I. Djurovich, B. D. Alleyne, M. Yousufuddin, N. N. Ho, J. C. Thomas, J. C. Peters, R. Bau, M. E. Thompson, *Inorg. Chem.* **2005**, *44*, 1713; b) M. K. Nazeeruddin, R. Humphry-Baker, D. Berner, S. Rivier, L. Zuppiroli, M. Graetzel, *J. Am. Chem. Soc.* **2003**, *125*, 8790; c) A. Tsuboyama, H. Iwawaki, M. Furugori, T. Mukaide, J. Kamatani, S. Igawa, T. Moriyama, S. Miura, T. Takiguchi, S. Okada, M. Hoshino, K. Ueno, *J. Am. Chem. Soc.* **2003**, *125*, 12971; d) A. B. Tamayo, B. D. Alleyne, P. I. Djurovich, S. Lamansky, I. Tsyba, N. N. Ho, R. Bau, M. E. Thompson, *J. Am. Chem. Soc.* **2003**, *125*, 7377; e) M. Sun, H. Xin, K.-Z. Wang, Y.-A. Zhang, L.-P. Jin, C.-H. Huang, *Chem. Commun.* **2003**, 702.

[2] a) M. C. DeRosa, D. J. Hodgson, G. D. Enright, B. Dawson, C. E. B. Evans, R. J. Crutchley, *J. Am. Chem. Soc.* **2004**, *126*, 7619; b) E. Mei, S. Vinogradov, R. M. Hochstrasser, *J. Am. Chem. Soc.* **2003**, *125*, 13198; c) R. Gao, D. G. Ho, B. Hernandez, M. Selke, D. Murphy, P. I. Djurovich, M. E. Thompson, *J. Am. Chem. Soc.* **2002**, *124*, 14828.

[3] a) S.-J. Yeh, W.-C. Wu, C.-T. Chen, Y.-H. Song, Y. Chi, M.-H. Ho, S.-F. Hsu, C.-H. Chen, *Adv. Mater.* **2005**, *17*, 285; b) J. Kavitha, S.-Y. Chang, Y. Chi, J.-K. Yu, Y.-H. Hu, P.-T. Chou, S.-M. Peng, G.-H. Lee, Y.-T. Tao, C.-H. Chien, A. J. Carty, *Adv. Funct. Mater.* **2005**, *15*, 223; c) X. Gong, J. C. Ostrowski, D. Moses, G. C. Bazan, A. J. Heeger, *Adv. Funct. Mater.* **2003**, *13*, 439; d) X. Gong, M. R. Robinson, J. C. Ostrowski, D. Moses, G. C. Bazan, A. J. Heeger, *Adv. Mater.* **2002**, *14*, 581; e) S. Lamansky, P. Djurovich, D. Murphy, F. Abdel-Razzaq, H.-E. Lee, C. Adachi, P. E. Burrows, S. R. Forrest, M. E. Thompson, *J. Am. Chem. Soc.* **2001**, *123*, 4304; f) P. Coppo, E. A. Plummer, L. De Cola, *Chem. Commun.* **2004**, 1774.

[4] a) M. A. Baldo, D. F. O'Brien, Y. You, A. Shoustikov, S. Sibley, M. E. Thompson, S. R. Forrest, *Nature* **1998**, *395*, 151; b) H. Yersin, *Top. Curr. Chem.* **2004**, *241*, 1.

[5] a) Y.-L. Tung, S.-W. Lee, Y. Chi, Y.-T. Tao, C.-H. Chien, Y.-M. Cheng, P.-T. Chou, S.-M. Peng, C.-S. Liu, *J. Mater. Chem.* **2005**, *15*, 460; b) H.-J. Su, F.-I. Wu, C.-F. Shu, Y.-L. Tung, Y. Chi, G.-H. Lee, *J. Polym. Sci. A: Polym. Chem.* **2005**, *43*, 859.

[6] a) P.-C. Wu, J.-K. Yu, Y.-H. Song, Y. Chi, P.-T. Chou, S.-M. Peng, G.-H. Lee, *Organometallics* **2003**, *22*, 4938; b) Y.-L. Tung, P.-C. Wu, C.-S. Liu, Y. Chi, J.-K. Yu, Y.-H. Hu, P.-T. Chou, S.-M. Peng, G.-H. Lee, Y. Tao, A. J. Carty, C.-F. Shu, F.-I. Wu, *Organometallics* **2004**, *23*, 3745; c) J.-K. Yu, Y.-H. Hu, Y.-M. Cheng, P.-T. Chou, S.-M. Peng, G.-H. Lee, A. J. Carty, Y.-L. Tung, S.-W. Lee, Y. Chi, C.-S. Liu, *Chem. Eur. J.* **2004**, *10*, 6255.

[7] Gaussian 03 (Revision C.02), M. J. Frisch, G. W. Trucks, H. B. Schlegel, G. E. Scuseria, M. A. Robb, J. R. Cheeseman, Jr., J. A. Montgomery, T. Vreven, K. N. Kudin, J. C. Burant, J. M. Millam, S. S. Iyengar, J. Tomasi, V. Barone, B. Mennucci, M. Cossi, G. Scalmani, N. Rega, G. A. Petersson, H. Nakatsuji, M. Hada, M. Ehara, K. Toyota, R. Fukuda, J. Hasegawa, M. Ishida, T. Nakajima, Y. Honda, O. Kitao, H. Nakai, M. Klene, X. Li, J. E. Knox, H. P. Hratchian, J. B. Cross, V. Bakken, C. Adamo, J. Jaramillo, R. Gomperts, R. E. Stratmann, O. Yazyev, A. J. Austin, R. Cammi, C. Pomelli, J. W. Ochterski, P. Y. Ayala, K. Morokuma, G. A. Voth, P. Salvador, J. J. Dannenberg, V. G. Zakrzewski, S. Dapprich, A. D. Daniels, M. C. Strain, O. Farkas, D. K. Malick, A. D. Rabuck, K. Raghavachari, J. B. Foresman, J. V. Ortiz, Q. Cui, A. G. Baboul, S. Clifford, J. Cioslowski, B. B. Stefanov, G. Liu, A. Liashenko, P. Piskorz, I. Komaromi, R. L. Martin, D. J. Fox, T. Keith, M. A. Al-Laham, C. Y. Peng, A. Nanayakkara, M. Challacombe, P. M. W. Gill, B. Johnson, W. Chen, M. W. Wong, C. Gonzalez, J. A. Pople, Gaussian, Inc., Wallingford, CT, **2004**.

[8] A. D. Becke, *J. Chem. Phys.* **1993**, *98*, 5648.

[9] C. Lee, W. Yang, R. G. Parr, *Phys. Rev. B* **1988**, *37*, 785.

[10] T. H. Dunning, Jr., P. J. Hay in *Modern Theoretical Chemistry* (Ed.: H. F. Schaefer, III), Plenum Press, New York, **1976**, vol. 3, p. 1.

[11] a) P. J. Hay, W. R. Wadt, *J. Chem. Phys.* **1985**, *82*, 270; b) W. R. Wadt, P. J. Hay, *J. Chem. Phys.* **1985**, *82*, 284; c) P. J. Hay, W. R. Wadt, *J. Chem. Phys.* **1985**, *82*, 299.

[12] P. C. Hariharan, J. A. Pople, *Mol. Phys.* **1974**, *27*, 209.

[13] a) G. D. Fasman, *Handbook of Biochemistry and Molecular Biology, Physical and Chemical Data*, 3rd. ed. CRC Press, Cleveland, OH, **1976**, vol. 1; b) K. Sakata, M. Hashimoto, H. Yoshino, *Inorg. Chim. Acta* **1985**, *99*, 231.

[14] M. S. A. Hamza, J. M. Pratt, *J. Chem. Soc., Dalton Trans.* **1993**, 1647.

[15] a) C. Lopez, S. Alvarez, X. Solans, M. Font-Bardia, *Polyhedron* **1992**, *11*, 1637; b) B. D. Gupta, V. Singh, R. Yamuna, T. Barclay, W. Cordes, *Organometallics* **2003**, *22*, 2670.

[16] C. M. Che, T. F. Lai, W. C. Chung, W. P. Schaefer, H. B. Gray, *Inorg. Chem.* **1987**, *26*, 3907.
[17] R. Salzmann, C. J. Ziegler, N. Godbout, M. T. McMahon, K. S. Suslick, E. Oldfield, *J. Am. Chem. Soc.* **1998**, *120*, 11323.
[18] a) A. Vogler, H. Kunkely, *Coord. Chem. Rev.* **2000**, *200–202*, 991; b) A. Vogler, H. Kunkely, *Top. Curr. Chem.* **2001**, *213*, 143.
[19] T. A. Perkins, D. B. Pourreau, T. L. Netzel, K. S. Schanze, *J. Phys. Chem.* **1989**, *93*, 4511.
[20] J.-K. Yu, Y.-M. Cheng, Y.-H. Hu, P.-T. Chou, Y.-L. Chen, S.-W. Lee, Y. Chi, *J. Phys. Chem. B* **2004**, *108*, 19908.
[21] a) M. A. Mansour, W. B. Connick, R. J. Lachicotte, H. J. Gysling, R. Eisenberg, *J. Am. Chem. Soc.* **1998**, *120*, 1329; b) E. Cariati, X. Bu, P. C. Ford, *Chem. Mater.* **2000**, *12*, 3385; c) R. L. White-Morris, M. M. Olmstead, F. Jiang, D. S. Tinti, A. L. Balch, *J. Am. Chem. Soc.* **2002**, *124*, 2327; d) E. J. Fernandez, J. M. Lopez-de-Luzuriaga, M. Monge, M. E. Olmos, J. Perez, A. Laguna, A. A. Mohamed, J. P. Fackler, Jr., *J. Am. Chem. Soc.* **2003**, *125*, 2022; e) H. V. R. Dias, H. V. K. Diyabalanage, M. A. Rawashdeh-Omary, M. A. Franzman, M. A. Omary, *J. Am. Chem. Soc.* **2003**, *125*, 12072; f) I. E. Pomestchenko, F. N. Castellano, *J. Phys. Chem. A* **2004**, *108*, 3485.
[22] J. R. Lakowicz, *Principles of Fluorescence Spectroscopy*, 2nd ed., Kluwer Academic, New York, **1999**.
[23] M. Polson, M. Ravaglia, S. Fracasso, M. Garavelli, F. Scandola, *Inorg. Chem.* **2005**, *44*, 1282.
[24] a) L. Yang, A.-M. Ren, J.-K. Feng, X.-D. Liu, Y.-G. Ma, H.-X. Zhang, *Inorg. Chem.* **2004**, *43*, 5961; b) E. Wolcan, G. Torchia, J. Tocho, O. E. Piro, P. Juliarena, G. Ruiz, M. R. Feliz, *J. Chem. Soc. Dalton Trans.* **2002**, 2194; c) A. Gabrielsson, S. Zalis, P. Matousek, M. Towrie, A. Vlcek, Jr., *Inorg. Chem.* **2004**, *43*, 7380.
[25] a) F. Neve, M. La Deda, A. Crispini, A. Bellusci, F. Puntoriero, S. Campagna, *Organometallics* **2004**, *23*, 5856; b) Q.-Z. Yang, Q.-X. Tong, L.-Z. Wu, Z.-X. Wu, L.-P. Zhang, C.-H. Tung, *Eur. J. Inorg. Chem.* **2004**, 1948.
[26] a) C.-C. Cheng, W.-S. Yu, P.-T. Chou, S.-M. Peng, G.-H. Lee, P.-C. Wu, Y.-H. Song, Y. Chi, *Chem. Commun.* **2003**, 2628; b) H.-Y. Chen, Y. Chi, C.-S. Liu, J.-K. Yu, K.-S. Chen, P.-T. Chou, S.-M. Peng, G.-H. Lee, A. J. Carty, S.-J. Yeh, C.-T. Chen, *Adv. Funct. Mater.* **2005**, *15*, 567.

Received: April 18, 2005
Published online: August 5, 2005

